Simultaneous broadband light trapping and fill factor enhancement in crystalline silicon solar cells induced by Ag nanoparticles and nanoshells

Narges F. Fahim,[1] Baohua Jia,[1,3] Zhengrong Shi,[2] and Min Gu[1,*]

[1]*Centre for Micro-Photonics, Faculty of Engineering and Industrial Sciences, Swinburne University of Technology, Hawthorn, 3122 Victoria, Australia*

[2]*Suntech Power Holdings Co., Ltd., 9 Xinhua Road, New District, Wuxi, Jiangsu Province 214028, China*

[3]*bjia@swin.edu.au*

[*]*mgu@swin.edu.au*

Abstract: Crystalline silicon solar cells are predominant and occupying more than 89% of the global solar photovoltaic market. Despite the boom of the innovative solar technologies, few can provide a low-cost radical solution to dramatically boost the efficiency of crystalline silicon solar cells, which has reached plateau in the past ten years. Here, we present a novel strategy to simultaneously achieve dramatic enhancement in the short-circuit current and the fill factor through the integration of Ag plasmonic nanoparticles and nanoshells on the antireflection coating and the screen-printed fingers of monocrystalline silicon solar cells, respectively, by a single step and scalable modified electroless displacement method. As a consequence, up to 35.2% enhancement in the energy conversion efficiency has been achieved due to the plasmonic broadband light trapping and the significant reduction in the series resistance. More importantly, this method can further increase the efficiency of the best performing textured solar cells from 18.3% to 19.2%, producing the highest efficiency cells exceeding the state-of-the-art efficiency of the standard screen-printed solar cells. The dual functions of the Ag nanostructures, reported for the first time here, present a clear contrast to the previous works, where plasmonic nanostructures were integrated into solar cells to achieve the short-circuit current enhancement predominately. Our method offers a facile, cost-effective and scalable pathway for metallic nanostructures to be used to dramatically boost the overall efficiency of the optically thick crystalline silicon solar cells.

OCIS codes: (040.5350) Photovoltaics; (250.5403) Plasmonics; (310.6628) Subwavelength structure, nanostructures; (160.5140) Photo conductive material; (160.4236) Nanomaterials.

References and links

1. D. H. Neuhaus and A. Munzer, "Industrial silicon wafer solar cells," Adv. Optoelectron. **2007**, 1–15 (2007).
2. Z. Wang, P. Han, H. Lu, H. Qian, L. Chen, Q. Meng, N. Tang, F. Gao, Y. Jia, J. Wu, Y. Fei, W. Wu, H. Zhu, J. Ji, Z. Shi, A. Sugianto, L. Mai, B. Hallam, and S. Wenham, "Advanced PERC and PERL production cells with 20.3% record efficiency for standard commercial p-type silicon wafers," Prog. Photovolt. Res. Appl. **20**(3), 260–268 (2012).
3. J. Zhao, A. Wang, and M. A. Green, "High-efficiency PERL and PERT silicon solar cells on FZ and MCZ substrates," Sol. Energy Mater. Sol. Cells **65**(1-4), 429–435 (2001).
4. A. Polman and H. A. Atwater, "Photonic design principles for ultrahigh-efficiency photovoltaics," Nat. Mater. **11**(3), 174–177 (2012).
5. H. A. Atwater and A. Polman, "Plasmonics for improved photovoltaic devices," Nat. Mater. **9**(3), 205–213 (2010).
6. H. R. Stuart and D. G. Hall, "Island size effects in nanoparticle-enhanced photodetectors," Appl. Phys. Lett. **73**(26), 3815–3817 (1998).

#172121 - $15.00 USD Received 6 Jul 2012; revised 10 Aug 2012; accepted 13 Aug 2012; published 16 Aug 2012

7. S. Pillai, K. R. Catchpole, T. Trupke, and M. A. Green, "Surface plasmon enhanced silicon solar cells," J. Appl. Phys. **101**(9), 093105 (2007).
8. S. H. Lim, W. Mar, P. Matheu, D. Derkacs, and E. T. Yu, "Photocurrent spectroscopy of optical absorption enhancement in silicon photodiodes via scattering from surface plasmon polaritons in gold nanoparticles," J. Appl. Phys. **101**(10), 104309 (2007).
9. K. Nakayama, K. Tanabe, and H. A. Atwater, "Plasmonic nanoparticle enhanced light absorption in GaAs solar cells," Appl. Phys. Lett. **93**(12), 121904 (2008).
10. R. A. Pala, J. White, E. Barnard, J. Liu, and M. L. Brongersma, "Design of Plasmonic thin-film solar cells with broadband absorption enhancements," Adv. Mater. (Deerfield Beach Fla.) **21**(34), 3504–3509 (2009).
11. S. Mokkapati, F. J. Beck, A. Polman, and K. R. Catchpole, "Designing periodic arrays of metal nanoparticles for light-trapping applications in solar cells," Appl. Phys. Lett. **95**(5), 053115 (2009).
12. N. C. Panoiu and R. M. Osgood, Jr., "Enhanced optical absorption for photovoltaics via excitation of waveguide and plasmon-polariton modes," Opt. Lett. **32**(19), 2825–2827 (2007).
13. K. R. Catchpole and A. Polman, "Design principles for particle plasmon enhanced solar cells," Appl. Phys. Lett. **93**(19), 191113 (2008).
14. F. J. Beck, A. Polman, and K. R. Catchpole, "Tunable light trapping for solar cells using localized surface plasmons," J. Appl. Phys. **105**(11), 114310 (2009).
15. D. Duche, P. Torchio, L. Escoubas, F. Monestier, J. J. Simon, F. Flory, and G. Mathian, "Improving light absorption in organic solar cells by plasmonic contribution," Sol. Energy Mater. Sol. Cells **93**(8), 1377–1382 (2009).
16. N. F. Fahim, Z. Ouyang, Y. Zhang, B. Jia, Z. Shi, and M. Gu, "Efficiency enhancement of screen-printed multicrystalline silicon solar cells by integrating gold nanoparticles via a dip coating process," Opt. Mater. Express **2**(2), 190–204 (2012).
17. T. L. Temple, G. D. K. Mahanama, H. S. Reehal, and D. M. Bagnall, "Influence of localized surface plasmon excitation in silver nanoparticles on the performance of silicon solar cells," Sol. Energy Mater. Sol. Cells **93**(11), 1978–1985 (2009).
18. F. J. Beck, S. Mokkapati, and K. R. Catchpole, "Designing periodic arrays of metal nanoparticles for light-trapping applications in solar cells," Prog. Photovolt. Res. Appl. **18**, 500–504 (2010).
19. X. Chen, B. Jia, J. K. Saha, B. Cai, N. Stokes, Q. Qiao, Y. Wang, Z. Shi, and M. Gu, "Broadband enhancement in thin-film amorphous silicon solar cells enabled by nucleated silver nanoparticles," Nano Lett. **12**(5), 2187–2192 (2012).
20. M. Hörteis, J. Bartsch, S. Binder, A. Filipovic, J. Merkel, V. Radtke, and S. W. Glunz, "Electrical properties of fine line printed and light-induced plated contacts on silicon solar cells," Prog. Photovolt. Res. Appl. **18**, 240–248 (2010).
21. H. Dong, R. Barr, and P. hinkley, "Inkjet plating resist for improved cell efficiency," *in proceedings of Photovoltaic Specialists Conference (PVSC) 35th IEEE 2010*, 002142–002146.
22. N. Bay, G. Cimiotti, S. Kleinschmidt, N. Kösterke, A. Lösel, M. Sailer, A. Träger, H. Kühnlein, H. Nussbaumer, C. Fleischmann, and F. Granek, "Industrial LCP selective emitter solar cells with plated contacts," *in proceedings of Photovoltaic Specialists Conference (PVSC) 35th IEEE 2010*, 000667–000671.
23. T. Nychyporuk, Z. Zhou, A. Fave, M. Lemiti, and S. Bastide, "Electroless deposition of Ag nanoparticles on the surface of SiNx: H dielectric layers," Sol. Energy Mater. Sol. Cells **94**(12), 2314–2317 (2010).
24. A. E. Ershov, I. L. Isaev, P. N. Semina, V. A. Markel, and S. V. Karpov, "Effects of size polydispersity on the extinction spectra of colloidal nanoparticle aggregates," Phys. Rev. B **85**(4), 045421 (2012).
25. Z. Ouyang, X. Zhao, S. Varlamov, Y. Tao, J. Wong, and S. Pillai, "Nanoparticle-enhanced light trapping in thin-film silicon solar cells," Prog. Photovolt: Res. Appl. **19**(8), 917–926 (2011).
26. M. A. Green, "Ag requirements for silicon wafer-based solar cells," Prog. Photovolt. Res. Appl. **19**(8), 911–916 (2011).
27. J. A. Silva, M. Gauthier, C. Boulord, C. Oliver, A. Kaminski, B. Semmache, and M. Lemiti, "Improving front contacts of n-type solar cells," Energy Procedia **8**, 625–634 (2011).

1. Introduction

Crystalline silicon solar cells dominate the photovoltaic market; nevertheless, due to the optical and electrical losses, the industrial achievable efficiencies of 10-18% [1, 2] are much lower than the laboratory best efficiency of 25% [3] and also far less than the predicted thermodynamic photovoltaic energy conversion efficiency [4]. Recently, plasmonic effects have emerged as a promising pathway to dramatically enhance the performance of solar cells [5–18]. Through integrating metallic nano-materials/structures into solar cells, the light trapping properties are greatly improved leading to significant photocurrent enhancement. Despite the impressive successes of the plasmonic effect in optically thin solar cells [19], the attempts in the optically thick solar cells, in particular the market dominant crystalline silicon solar cells, are limited but is obviously of great significance for photovoltaic industry. To make the metallic nano-materials/structures effective in the crystalline silicon solar cells, two

#172121 - $15.00 USD Received 6 Jul 2012; revised 10 Aug 2012; accepted 13 Aug 2012; published 16 Aug 2012

key challenges have to be addressed. The first one is the broadband light trapping by the nano-materials/structures. It is known that crystalline silicon solar cells possess broadband absorption from 400 to 1100 nm. The narrow band light trapping enhancement induced by the resonant plasmonic effect can hardly lead to any obvious photocurrent enhancement of crystalline silicon solar cells. The second challenge is to find new enhancement mechanisms enabled by the nano-materials/structures beyond the light trapping. The large thickness of crystalline silicon solar cells (180-300 μm) has made them a good solar light absorber. Thus further optimization in light trapping can only lead to marginal photocurrent enhancement. Therefore, to achieve large overall energy conversion efficiency (η) improvement, a new enhancement mechanism is required.

Here, we propose and demonstrate an innovative strategy to concurrently achieve broadband light trapping and series resistance (R_s) reduction in crystalline silicon solar cells by simultaneously depositing Ag nanoparticles (NPs) on the SiN_x antireflection coating (ARC) and Ag nanoshells on the screen-printed fingers using a single-step modified electroless deposition method. Our strategy not only leads to the large enhancement in the short-circuit current (J_{sc}) but also boosts significantly the fill factor (FF) in the meantime. To examine the effectiveness of this method, two groups of screen-printed solar cell (dominant product on the market) samples have been investigated in this paper. The first group is planar solar cells without the front-surface texture. A massive 35.2% increase in the energy conversion efficiency has been achieved proving that this method can function as an effective alternative for the conventional surface texturing. The second group is the standard textured solar cells. Our systematic study has shown that this simple method can consistently and significantly improve the efficiency of all the textured cells investigated in the second group. In particular, it can dramatically enhance the efficiency of the best performing cells to 19.2% much exceeding the state-of-the-art efficiency value (17.8%) of the standard screen-printed solar cells [1, 2].

2. Experimental methods

2.1. Ag electroless deposition on solar cells

To better scrutinize the light trapping effect screen-printed planar monocrystalline silicon solar cells (Suntech Power Holdings Co., Ltd.) without any surface texturing were first employed, as shown in Fig. 1(a). The cells were fabricated from the *p*-type Si wafer with *n*-type passivated emitter. The front Ag metal fingers, busbar and the Al/Ag back contact and Al back reflector were made by the screen-printing method [1]. All the planar solar cells, in this study, possess a SiN_x film as the ARC with a thickness of 107 nm and a refractive index (n) of 2.05 as measured by ellipsometry. Solar cells were cut into 2×2 cm^2 and degreased by immersion into an ethanol bath for 1 min, then blown dry with a stream of nitrogen. The electroless deposition of Ag NPs was performed by immersing the solar cells vertically in an acidified aqueous solution of silver nitrate (10^{-3} M $AgNO_3$ and 0.04 M HNO_3) for 5 to 20 min. The silver-deposited solar cells were then removed from the metal solution and washed with copious amount of deionised water. The surface was subsequently blown dry with a stream of nitrogen.

2.2. Photovoltaic and morphological characterization

The current density-voltage characteristics curves were measured using a solar simulator under the Air Mass 1.5 Global (AM 1.5G) illumination condition (100 mW/cm^2) calibrated by a reference silicon photodiode using a Newport solar simulator (Oriel Sol 3A^{TM} class AAA, model 94023A) and Keithley 2400 source meter. The external quantum efficiency (EQE) was measured using an AM 1.5G standard spectrum. The EQE spectrum was calculated as the ratio between spectral response data and the incident light spectrum, obtained by a reference Si photodiode (1F053). The EQE measurements were taken from 300 nm to 1100 nm. The

#172121 - $15.00 USD Received 6 Jul 2012; revised 10 Aug 2012; accepted 13 Aug 2012; published 16 Aug 2012

reflectance spectra of the solar cells were recorded using an integrated sphere of UV–VIS–NIR spectrophotometer (Perkin Elmer, Lambda 1050) for wavelengths ranging from 300 to 1100 nm. All solar cells were characterized before and after electroless deposition of Ag nanoparticles for the same photovoltaic cells. The thickness of SiN_x anti-reflection coating was measured by ellipsometry (J.A. Woollam M-2000XI).

In order to perform morphology and qualitative analysis, field emission scanning electron microscopy (FE-SEM) and energy dispersive x-ray spectroscopy (EDX) were employed with FEI Helios NanoLab 600i field emission scanning electron microscope. For cross-section preparation, the focus ion beam (FIB) method was used, which equipped in the same FE-SEM system. The mean diameter, size distribution and surface coverage were measured from several SEM micrographs using computer software.

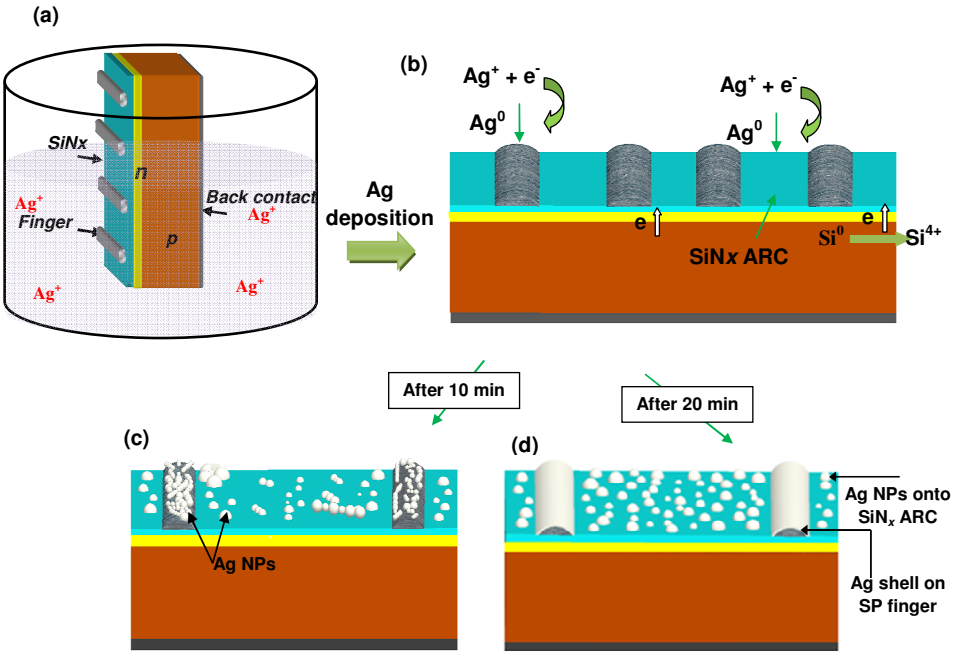

Fig. 1. Electroless deposition set-up and mechanism of simultaneous formation of Ag NPs and nanoshells. (a) Schematic diagram of the experimental set-up for Ag electroless deposition onto Si solar cells from the fluoride free solution. (b) Sketch shows the Ag NPs formation mechanism, the silver ions reduced by getting electrons from Si through Si nanoclusters, scratches, pinholes, and blisters in SiN_x ARC. (c) Formation of Ag NPs on the screen-printed (SP) fingers and SiN_x ARC after deposition for 10 min. (d) Formation of Ag nanoshells on the SP fingers and Ag NPs on SiN_x ARC after deposition for 20 min.

3. Results and discussion

The modified electroless deposition method used in our experiment, as illustrated in Fig. 1(a), is simple, cost-effective and of high throughput ready for large scale industry mass production. In conventional electroless deposition process two major issues exist. The first one is called the ghost plating phenomenon, which leads to the formation of large metallic particles of tens of micrometres in dimensions on the SiN_x ARC inducing shading losses, which reduce J_{sc} of the solar cells [20–23]. The second issue is the corrosion and metallic contamination of the cells by using hydrofluoric acid (HF), which is considered as a formidable barrier for application in photovoltaic solar cells, thereby deteriorating the cell electrical performance. We have solved these problems with the following methods. To produce nanometer sized metallic particles useful for light trapping, the electroless deposition process was conducted without any contact to the rear side of the solar cells. Therefore, the

#172121 - $15.00 USD Received 6 Jul 2012; revised 10 Aug 2012; accepted 13 Aug 2012; published 16 Aug 2012

absence of external electrical current, capping agents and reducing agents slows down the deposition rate and leads to the formation of NPs instead of micro-particles, thereby minimizing the shading loss. Thus a new role of ghost plating, which has long been regarded as undesirable and deliberately suppressed, can now lead to scattering NPs with desirable plasmonic properties to enhance the light absorption in solar cells. Second, the HF acid used for the acidification of metal salt was replaced by the HNO_3 acid thus the metallic contamination and corrosion problems are significantly alleviated and yielding cells with superior electrical properties. Metal NPs prepared by this electroless method exhibit excellent adhesion to the underlying substrate and their morphology can be tuned by controlling the electroless deposition parameters.

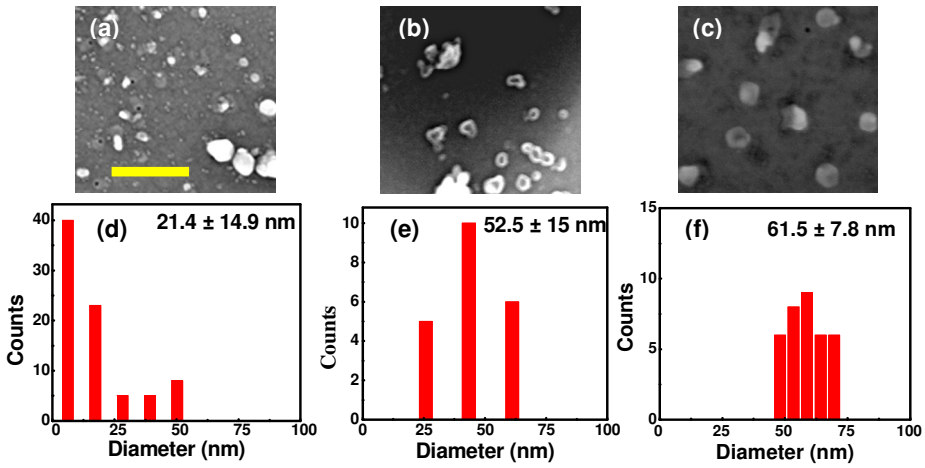

Fig. 2. SEM micrographs of Ag nanoparticles deposited by electroless deposition on the front surface of planar Si solar cells and their corresponding histograms (bottom) that show the statistical analysis of micrographs and the size distributions of (a) 21.4 nm, (b) 52.5 nm and (c) 61.5 nm. The surface coverage is 3, 3, and 6.9% for (a), (b), and (c), respectively. The scale bar is 200 nm.

The mechanism for the unequal deposition of Ag NPs on the ARC and fingers of solar cells is given in Figs. 1(b)-1(d). It can be explained in term of the nucleation sites as follows: (1) The driving force for the formation of Ag NPs on the SiN_x ARC is the presence of Si nanoclusters, pinholes, blisters and scratches in the SiN_x ARC, where the anodic oxidation of Si is coupled to the cathodic reduction of Ag^+ ion, which urges the formation of low density NPs (Figs. 1(b)-1(d)). This method is able to produce NPs with controlled sizes, which potentially enables broadband light trapping in solar cells. (2) On the other hand, the fingers contain screen-printed Ag layer that acts as a seed enhancing the deposition rate of Ag NPs, thereby a high density of nucleation sites. As a result, the Ag NPs grow in size with increasing the electroless deposition time and eventually merge to form homogeneous, smooth and dense metal nanoshell that completely encapsulates the spongy screen-printed fingers. It is expected that the conductivity of the nanoshelled metal contacts can be improved, which in turn increases the *FF*.

To find the optimized NPs for the light trapping effect, three particle sizes were employed based on the previous studies [17] by controlling the electroless deposition time. Figure 2 shows the field emission scanning electron microscopy (FESEM) images of the Ag NPs deposited electrolessly via the galvanic displacement on the SiN_x ARC of planar Si solar cells as a function of the deposition time of (a) 5 min, (b) 10 min, and (c) 20 min. It can be seen that the electroless deposition leads to the formation of predominately isolated Ag spherical particles with a limited number of clustered NPs randomly distributed on the surface of the

#172121 - $15.00 USD Received 6 Jul 2012; revised 10 Aug 2012; accepted 13 Aug 2012; published 16 Aug 2012

cell. Both the particle density and average particle diameter increase with the electroless deposition time. The average diameter of the particles increases from 21 nm after 5 min of deposition to 61.5 nm after 20 min. The particle size distributions are calculated from the SEM images and depicted in the corresponding histograms. The sizes are 21 ± 14.9, 52.5 ± 15 and 61.5 ± 7.8 nm for a deposition time of 5, 10 and 20 min, respectively. The fact that the electroless deposition results in a distribution of particle diameters indicates the silver phase formation is a continuous process (i.e. new nanoparticles are formed while old particles increase in diameter). This wide distribution in the particle size leads to broad and asymmetric surface plasmon resonance peaks, which have been confirmed to be favourable for broadband plasmonic light trapping [24, 25]. The corresponding surface coverage as a function of the deposition time is 3, 3, and 6.9% as estimated from the SEM images. The chemical composition of the deposited particles was confirmed by energy dispersive x-ray spectroscopy (EDX) measurement.

Figure 3(a) shows the SEM image of the finger after the electroless deposition of Ag. In clear contrast to the screen printed finger in Fig. 3(c), in which the particle-like porous front finger is presented, the electroless deposition results in the formation of nanoshell filling up and connecting the voids, which occupy about 20-30% of the fired paste [26] in the screen-printed finger. This underscores the importance of our electroless method in healing of small finger disruptions or constrictions. Such high quality Ag nanoshells are expected to dramatically improve the conductivity of the fingers. Further evidence for the formation of Ag nanoshells with a better quality and homogeneity onto the screen-printed fingers was confirmed by the cross-section FESEM images (Fig. 3(b)), in which the screen-printed fingers are clearly encapsulated by the nanoshell of Ag after the electroless deposition for 20 min. It is evident that there are two distinguishable layers. The electroless plated shell layer is smooth and dense, while the screen-printed core is rough and porous (with void indicated by the white arrow). The thickness of the Ag shell depends on the electroless deposition time, for a shorter time of 5-10 min, only Ag NPs can be formed on the fingers as illustrated in Fig. 1(c) and experimentally confirmed; while for a longer time (20 min), a thicker continuous Ag shell of thickness ranging from 475 to 800 nm is formed (Fig. 3(b)). The purity of the deposited Ag nanoshell on the screen-printed fingers was confirmed by the EDX measurement with the presence of Ag and Si peaks only. In comparison, the EDX spectrum of screen-printed fingers prior to the Ag shell formation (Fig. 3(d)), shows the presence of *Pb* peaks and other peaks due to the existence of the glass frit (typically lead borosilicate glass) which is responsible for the formation of an insulating glass layer beneath the finger. It is expected that the resistivity of a plated metal contact is much lower than that of a screen-printed one because pure metal is deposited during the electroless plating rather than metal pastes containing the organic binder and glass frit [20]. As a result, the series resistance is expected to be significantly reduced after the electroless plating process [27] leading to the *FF* improvement. Moreover, it has also been found that the front busbars contain Ag NPs after the electroless deposition, which, in turn, could further reduce the series resistance.

#172121 - $15.00 USD Received 6 Jul 2012; revised 10 Aug 2012; accepted 13 Aug 2012; published 16 Aug 2012

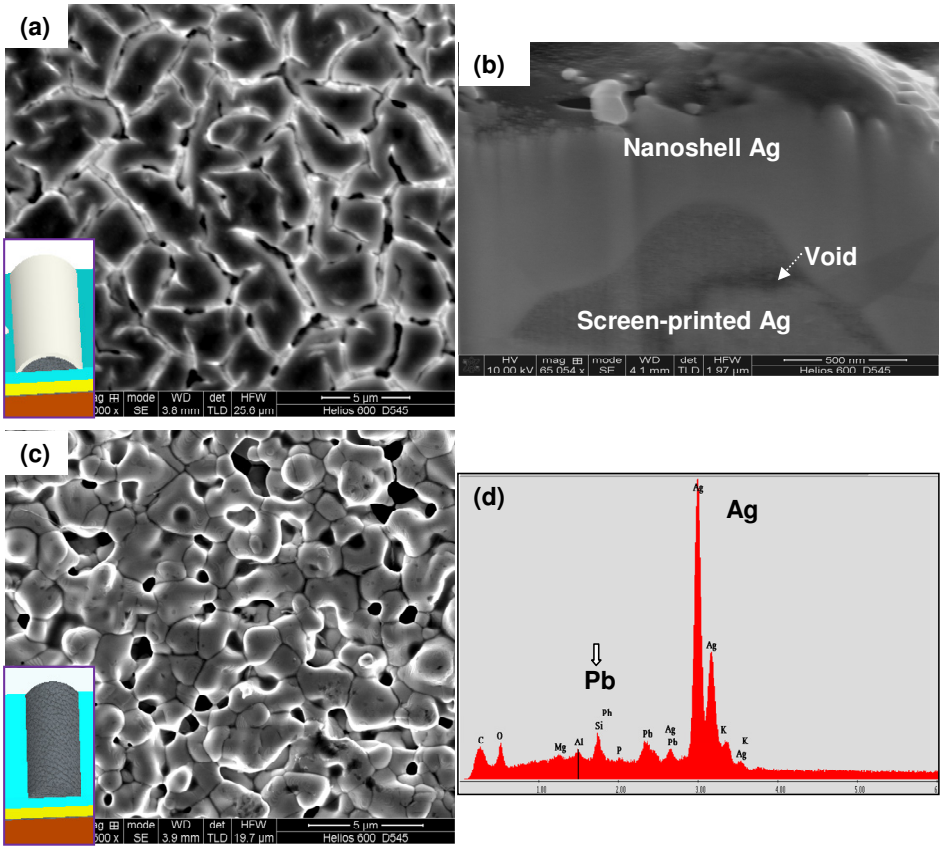

Fig. 3. SEM images of the fingers of the planar solar cells before and after the electroless Ag deposition. (a) SEM micrograph of the finger with the Ag nanoshell. The inset shows schematic diagram of the fingers with the Ag nanoshell. (b) SEM micrograph of the cross-section of the SP finger after the electroless deposition of Ag for 20 min. Two distinguishable layers can be identified, one smooth (i.e. no Ag clusters can be distinguished) corresponding to the Ag nanoshell that covers the finger and the rough one corresponding to the SP Ag. (c) SEM micrograph of spongy SP front-finger prior to the Ag electroless deposition for comparison. The inset show schematic diagram of the SP fingers before the deposition of Ag shell (d) EDX spectrum of the fingers prior to the Ag shell formation, it is evident that the presence of Pb peaks due to the presence of glass frit (*typically lead borosilicate glass*) in the SP Ag fingers.

The effect of the NPs on the light trapping of solar cells can be probed by the optical reflection properties and the external quantum efficiency (EQE) before and after the electroless deposition of Ag NPs with mean diameters of 21, 52.5 and 61.5 nm as shown in Figs. 4(a)-4(d). The reflectance and EQE curves of the pristine Si solar cell before the electroless Ag deposition are given in Fig. 4(a). The relative reflectance plots that have been normalized to the pristine cells are shown in Fig. 4(b). It is evident that the reflectance was reduced over broad wavelengths from 430 to 743 nm with an obvious dip of 7.3% centred at 600 nm when Ag NPs of mean diameter of 61.5 nm were deposited on the ARC surface of the cells. This reduction is attributed to the silver NPs induced forward-scattering, which increases the path length in the silicon active layer, since the reduction occurs close to the peak wavelength of the surface plasmon resonance (SPR) of the NPs. The increase in the surface reflectance at the longer wavelengths greater than 743 nm, for all cells, is most likely attributed to the back-scattering by the NPs [17].

#172121 - $15.00 USD Received 6 Jul 2012; revised 10 Aug 2012; accepted 13 Aug 2012; published 16 Aug 2012

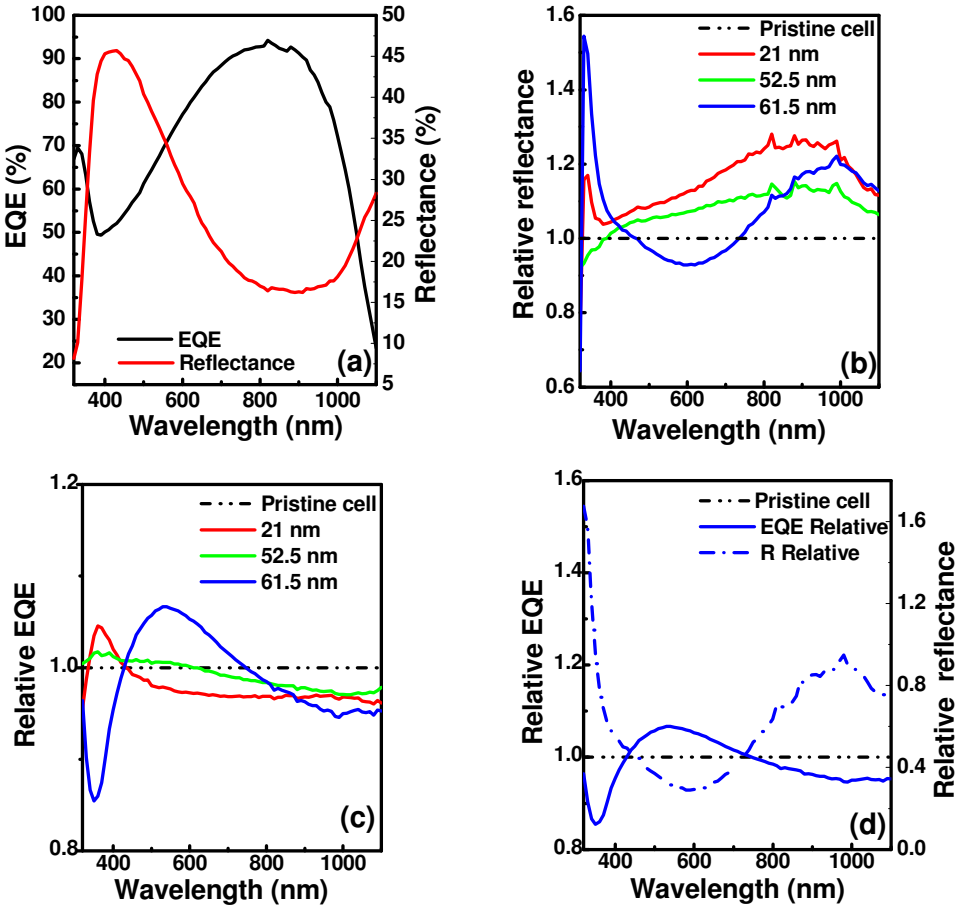

Fig. 4. The optical properties and the EQE performance of planar Si solar cells before and after electroless Ag deposition. (a) EQE and reflectance of the pristine solar cell before the Ag electroless deposition. (b) Relative reflectance normalized to the pristine cell and cells with Ag NPs of average sizes 21, 52.5, and 61.5 nm. (c) Relative EQE of cells with the Ag NPs of average size of 21, 52.5, and 61.5 nm normalized to the pristine cell. (d) Relative EQE and reflectance of the solar cells with Ag NPs of an average size of 61.5 nm.

The origin of the reduction in the cell reflectance after the electroless deposition of Ag NPs of size 61.5 nm can be further scrutinized by the measurement of the EQE of the solar cells. Importantly, the EQE measurement is more relevant than the absorption measurement of the solar cells for determining the enhancement in the cell absorption because it can decouple the light absorption in the active layer from the parasitic absorption caused by the silver NPs. It can be seen from Fig. 4(c), where the relative EQE plots are presented, the EQE for the cell coated with Ag NPs of size 61.5 nm was enhanced by 6.7% over a broad spectral range from 430 to 743 nm with a pronounced peak centred at approximately 538 nm. The increase in EQE indicates that the Ag NPs can strongly enhance the absorption in the photoactive layer and hence lead to the increase in the photocurrent. The slight decrease in the EQE outside the wavelengths range of 430-743 nm can be attributed to the back-scattering effect [17]. For the cells incorporating 52.5 nm Ag NPs, the small reduction of reflectance at the short wavelengths results in a modest increase in the EQE at wavelength ranging from 350 to 690 nm, while the EQE of cells with 21.5 nm Ag NPs show dominate decrease due to the parasitic absorption by NPs. We have found that further increasing the particle size causes a

#172121 - $15.00 USD Received 6 Jul 2012; revised 10 Aug 2012; accepted 13 Aug 2012; published 16 Aug 2012

reduction in the observed photocurrent enhancement, likely due to the excitation of multipole oscillations [6]. Therefore the particle size should be tailored carefully to minimize the back-scattering and parasitic absorption in metal NPs.

The relative reflectance and EQE of the cells coated with 61.5 nm Ag NPs, normalized to the pristine cell, are shown in Fig. 4(d). A clear correlation between the reflectance and the EQE is evident with an increase in reflectance resulting in a decrease in EQE at wavelength below 400 nm. Furthermore, the large reduction of reflectance over spectral range from 430 to 743 nm results in a substantial increase in EQE at exactly the same spectral range. The mechanism behind this effect is the forward-scattering of light by the quadrupolar mode, which redirects the light preferentially into the higher refractive index solar cells [12, 17]. At the longer wavelengths of $\lambda > 750$ nm a decrease of EQE was observed due to an increase in the back-scattering.

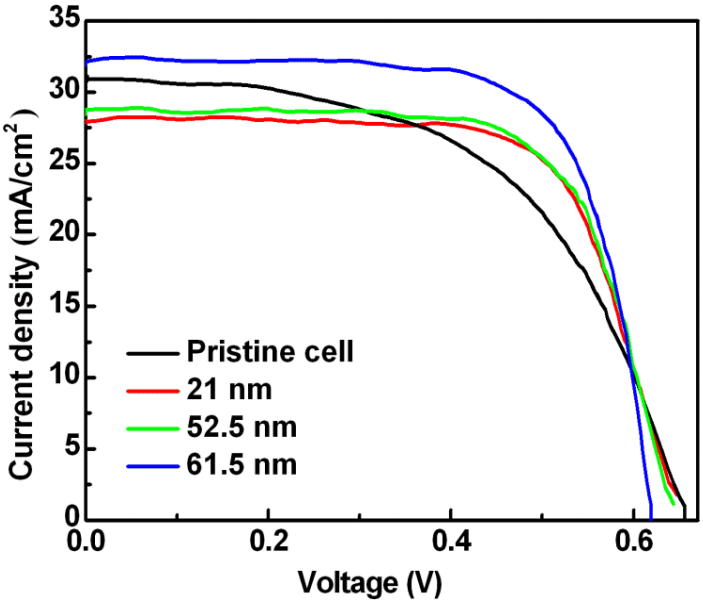

Fig. 5. Current density-voltage characteristic curves of planar silicon solar cell before and after the electroless deposition of Ag NPs of average particle sizes of 21, 52.5, and 61.5 nm.

Figure 5 shows the current density-voltage characteristic curves of the solar cells before and after the electroless deposition of Ag NPs on the front surface, which unambiguously confirm the effectiveness of NP scattering in improving J_{sc} and η of the solar cells. As expected, the largest enhancement was achieved by the Ag NPs of mean diameter 61.5 nm with 4% relative increase in J_{sc} from 31.1 to 32.3 mA/cm^2, which is consistent with the reflectance reduction and EQE enhancement presented in Fig. 4. Thus it has been confirmed that the broadband light trapping induced by the 61.5 nm Ag NPs has been achieved.

As expected, in Fig. 5 the *FF* of the solar cells incorporating the Ag NPs shows an obvious improvement comparing to that of the pristine cells. To quantify the improvement, Table 1 lists the variation of the open circuit voltage (V_{oc}), J_{sc}, *FF* and η before and after the electroless Ag deposition. Massive improvement in the *FF* has been achieved for all the cells. Particularly for the solar cells with the Ag NPs of size 61.5 nm the *FF* improves from 56.4% to 76%, which represent a remarkable 34.8% enhancement. This can be attributed to the significant reduction in the series resistance from 8.9 Ω/cm^2 to 1.4 Ω/cm^2 confirming the

#172121 - $15.00 USD Received 6 Jul 2012; revised 10 Aug 2012; accepted 13 Aug 2012; published 16 Aug 2012

positive effect of the nanoshells in improving the conductivity of the contact. A small decrease can be observed in V_{oc} for all cells after electroless process, which might due to the increased recombination as the Ag metal is in direct contact with Si. For cells with Ag NPs of sizes 21 and 52.5 nm, J_{sc} was reduced, but as long as the decrease of J_{sc} is compensated by the *FF* increase, the overall cell efficiency still rises. The pristine Si solar cell initially had an absolute efficiency of 11.2%, which was substantially increased to 15.2% after depositing the 61.5 nm Ag NPs electrolessly. This massive increase is clearly due to the concurrent improvement in J_{sc} and *FF*, which is a direct consequence of the broadband light trapping and the series resistance reduction induced by Ag NPs and nanoshells. The results demonstrate that the electroless deposition of Ag NPs and nanoshells can be used as a simple and effective alternative to the conventional surface texturing process for solar cells, in particular for those cells that are difficult to form high quality textures, for example the multicrystalline and ultra-thin silicon wafer solar cells.

Table 1. Summary of current density-voltage photovoltaic characteristics and energy conversion efficiency enhancement for planar silicon solar cells before and after electroless deposition of silver nanoparticles

Solar Cells	V_{oc} (mV)	J_{sc} (mA.cm^{-2})	*FF* (%)	R_s (Ω.cm^2)	η (%)	η Relative Enhancement (%)
Pristine *(as-received)*	655	31.1	56.4	8.9	11.2	N/A
Ag-21 nm	651.4	28.1	73.2	2.4	13.4	19.7
Ag-52.5 nm	643.5	28.5	73.6	2	13.5	20.2
Ag-61.5 nm	619	32.3	76	1.4	15.2	35.2

***V_{oc}*:** Open-circuit voltage, ***J_{sc}*:** Short-circuit current density, ***FF*:** fill factor, ***η*:** Energy conversion efficiency

To investigate the impact of our method on the high efficiency crystalline Si wafer solar cells, we performed deposition of Ag NPs on the highest available performance monocrystalline Si screen-printed solar cells with an initial efficiency 18.3%. These cells are made by the standard procedure from the production line with the SiN_x antireflection coating (90 nm) and the front surface texturing. Since the surface condition of the textured cells are significantly different from that of the planar cells, we performed another round of optimization for the Ag NP size. It has been found that the mean size of 55.5 ± 27.7 nm NPs provide the highest enhancement, as shown in Fig. 6. Due to the broadband light trapping (Figs. 6(a)-6(c)) and the reduced electrical loss, the J_{sc} is enhanced from 37.95 to 38.91 mA/cm^2 and the *FF* increases from 77.1% to 79.4%, respectively as shown in Fig. 6(d). In the meantime, the V_{oc} remains almost unchanged (from 0.623 to 0.620 V). Consequently the energy conversion efficiency is increased considerably from 18.3% to 19.2%, corresponding to a significant 4.9% enhancement compared to the same cell without NPs. It is worth mentioning that the 18.3% cells are among the best available screen-printed solar cells [2]. It is of great challenge to further increase even 1% of their efficiency by the conventional solar cell engineering methods. Apart from the capability of significantly increasing the almost perfect solar cells, our experiment has confirmed that this method is also able to consistently and repeatibly enhance the less performing cells (15-16%) with an even larger magnitude, upgrading them to become the normal (17%) or even high performance cells (>18%). This finding is of great significance to solar industry since the low performance solar cells are normally disposed to avoid the degradation of the overall output of the entire solar module.

#172121 - $15.00 USD Received 6 Jul 2012; revised 10 Aug 2012; accepted 13 Aug 2012; published 16 Aug 2012

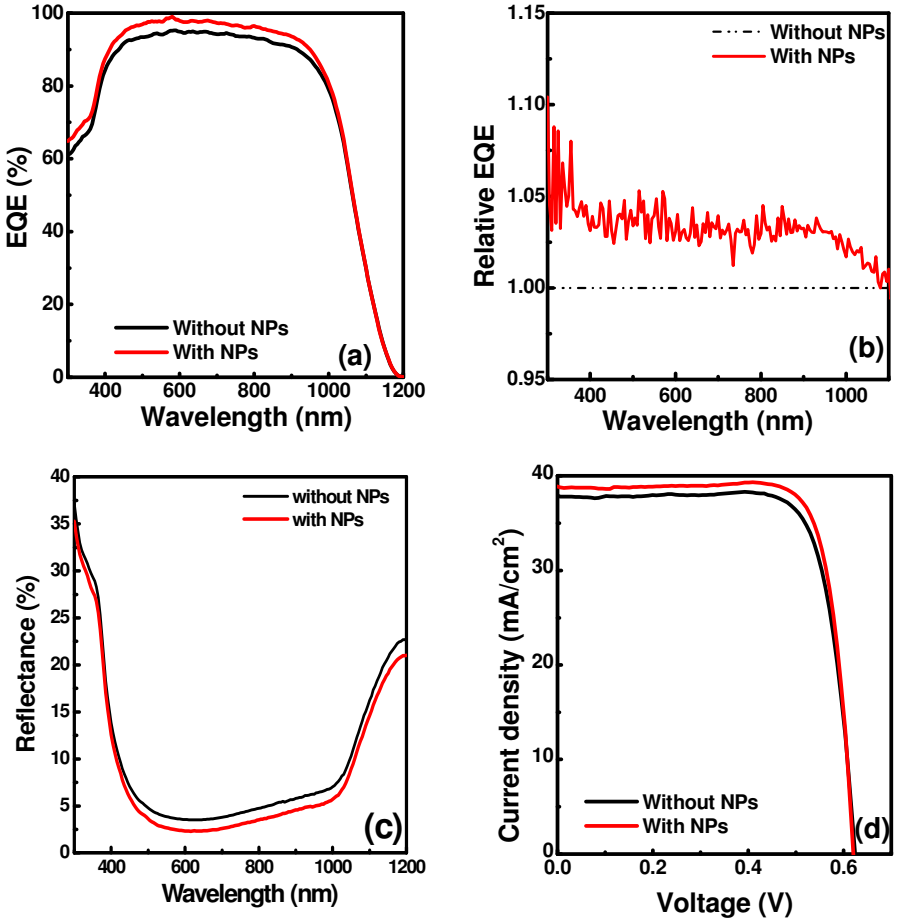

Fig. 6. External quantum efficiency (EQE) characteristics (a), Relative EQE (b), Reflectance (c), and IV curves (d) of high performance standard textured monocrystalline Si solar cell with and without Ag NPs of mean size 55.5 ± 27.7 nm on the same cell.

4. Conclusions

We have proposed and demonstrated an innovative approach to simultaneously improving the photocurrent generation and electrical performance of optically thick monocrystalline silicon screen-printed solar cells by concurrently depositing Ag NPs and nanoshells through a facile one-step modified electroless deposition method. It has been demonstrated that this method is highly effective for planar cells without surface texture, providing a low cost and environmentally-friendly alternative for the conventional surface texturing process, which includes corrosive strong acid or alkalis. For planar cells, the randomly distributed Ag NPs with tailored sizes on the surface of SiN_x ARC leads to obvious broadband light trapping over spectral wavelengths from 430 to 743 nm inside the silicon photoactive layer, matching well with the peak of the solar spectrum. Significant photocurrent enhancement of 4% (from 31 to 32.3 mA/cm^2) was demonstrated due to the plasmonic enhanced light scattering. The series resistance of the solar cells have been improved dramatically due to the simultaneous formation of the highly conductive Ag nanoshells encapsulating the fingers, which leads to the enormous enhancement of the *FF* from 56.4 to 76%. Consequently, the simultaneous

#172121 - $15.00 USD Received 6 Jul 2012; revised 10 Aug 2012; accepted 13 Aug 2012; published 16 Aug 2012

improvements in both the FF and J_{sc} lead to 35.2% relative enhancement in energy conversion efficiency of the planar solar cells. For standard textured solar cells, our method can upgrade the less performing solar cells to the normal or high performing group and thus narrowing the efficiency distribution of the entire group. More importantly, this method can further increase the efficiency of the best performing textured solar cells from 18.3% to 19.2%, producing the highest efficiency cells exceeding the state-of-the-art efficiency of the standard screen-printed solar cells. The novel approach presented in this paper provides a clear pathway for making the most of the metallic NPs to achieve unprecedented efficiency enhancement even in the optically thick silicon solar cells.

Acknowledgments

The authors acknowledge the financial support from the Victorian Government to establish the Victoria-Suntech Advanced Solar Facility (VSASF) under the Victoria Science Agenda (VSA) scheme. Baohua Jia thanks the Victorian Government for the support through the Victorian Fellowship.

#172121 - $15.00 USD Received 6 Jul 2012; revised 10 Aug 2012; accepted 13 Aug 2012; published 16 Aug 2012